Optimizing Electric Vehicle Steering Force Control using Slip Ratio Observer: Analysis and Comparison of Results on Matlab Simulink and CarSim

Thi Hoai Thu Anh An
Department of Electrical Engineering, University of Transport and Communications, Vietnam
htanh.ktd@utc.edu.vn

Anh Linh Pham
Department of Science and Technology, University of Transport and Communications, Vietnam
linhpkhcn@utc.edu.vn (corresponding author)

Received: 5 February 2025 | Revised: 26 February 2025 and 22 March 2025 | Accepted: 28 March 2025

 DOI: https://doi.org/10.48084/etasr.10462

ABSTRACT

This paper presents a control and torque distribution method for Electric Vehicles (EVs) based on a slip ratio observer. The EV model used is a four-wheel model, developed and simulated in two different software environments: Matlab Simulink and CarSim. In addition, the paper incorporates a slip ratio observer to achieve optimal results. Firstly, the slip ratio of the four wheels is observed to monitor and adjust the steering force, thereby regulating the vehicle dynamics to ensure stability under various road conditions and achieve optimal driving performance. Next, the vehicle model is implemented in both software environments to compare and evaluate the differences in control effectiveness, accuracy, and simulation capabilities between the two tools. Finally, the simulation results from both software platforms are analyzed to provide valuable insights for selecting an appropriate simulation approach in the design and development of EVs, as well as to validate the effectiveness of the proposed slip ratio observation method.

Keywords-EV; slip ratio; traction control; traction distribution; CarSim

I. INTRODUCTION

Electric Vehicles (EVs) are increasingly becoming the primary development trend in the automotive industry due to their outstanding advantages in energy efficiency and environmental emission reduction [1-3]. Therefore, many studies have been conducted on EVs [4-11]. However, steering force control and distribution in these vehicles still face many challenges, especially those related to road grip and vehicle stability under complex driving conditions. The steering force control system ensures safety and optimizes operating performance [12-14]. When the vehicle enters a slippery road, the traction coefficient is low, and the slip ratio of each wheel will increase sharply, causing dangerous phenomena such as loss of vehicle control and swaying when turning. To limit this undesirable behavior, it is necessary to observe and estimate the slip ratio, which is a complicated quantity to measure accurately. The EV model used in this article is a four-wheel independent vehicle model [15-16], and CarSim software is used to build the most realistic model and dynamics [17-18].

In the linear motion of EVs, authors in [19] used a slip mode controller in the wheel anti-slip system to improve traction. As the car accelerated, the amount of energy consumed could be reduced. Authors in [20] and [21] adopted the sliding mode control method and combined Direct Yaw Control (DYC) with steering control, and realized the separation of yaw rate and side slip angle by introducing the steering angle control parameter. Authors in [22] and [23] monitored the side slip angle and designed corresponding correction factors to correct the rotational speed error. Authors in [24] presented an Accelerated Slip Adjustment (ASR) system for EVs, which was introduced with three main control methods: torque balancing between axles, optimizing torque distribution between axles, and independently controlling the sliding speed. The simulation results demonstrate that the proposed ASR system effectively utilizes road surface friction and minimizes wheel slippage, while significantly improving the vehicle's longitudinal movement stability.

This paper will build a slip ratio observer to improve vehicle stability on all types of roads, and build a vehicle model on both Matlab Simulink and CarSim to compare the difference

between the simulation results obtained from the two software, identify the advantages and limitations of each software, and choose the appropriate software for each stage of the research process. Finally, the simulation results will demonstrate the correctness and effectiveness of the proposed software.

II. ELECTRIC VEHICLE MODELING

Figure 1 shows the structure of the four-wheel EV model, where δ_i^*, T_i^*, T_{bi}^* are the steering angle, applied moment, and braking moment, respectively, and r, v_x, and v_y are the angular velocity, longitudinal velocity, and transverse velocity of the Center of Gravity (COG).

A. Dynamic Model

Figure 2 shows the forces acting on the vehicle and wheels, the coordinate system, and the geometrical parameters of the vehicle. To clearly analyze the vehicle dynamics components, we need to determine the following equations: the force and moment balance model, the steering angle distribution, the relationship between the trunnion ratio and the friction coefficient, the wheel velocity, the forces acting on the wheels, and the regular forces.

Applying Newton's second law to Figure 2, we get:

$$\begin{cases} ma_x = \left(F_{x1}\cos\delta_1 + F_{x2}\cos\delta_2\right) \\ -\left(F_{y1}\sin\delta_1 + F_{y2}\sin\delta_2\right) + F_{x3} + F_{x4} - F_{res} \\ ma_y = \left(F_{x1}\sin\delta_1 + F_{x2}\sin\delta_2\right) \\ -\left(F_{y1}\cos\delta_1 + F_{y2}\cos\delta_2\right) + F_{y3} + F_{y4} \\ J_z\dot{r} = \left(l_f F_{x1}\sin\delta_1 + l_f F_{x2}\sin\delta_2\right) \\ +\left(l_f F_{y1}\cos\delta_1 + l_f F_{y2}\cos\delta_2\right) - l_f\left(F_{y3} + F_{y4}\right) \\ -0.5b_f\left(F_{x1}\cos\delta_1 + F_{x2}\cos\delta_2\right) \\ +0.5b_f\left(F_{y1}\sin\delta_1 - F_{y2}\sin\delta_2\right) - 0.5b_r\left(F_{y3} - F_{y4}\right) \end{cases} \quad (1)$$

$$F_{res} = F_{air} + F_{roll} = C_d A_F \frac{\rho}{2} v_x^2 + c_{rr} mg \quad (2)$$

where m is the mass of the vehicle, J_z is the moment of inertia around the z-axis, F_{xi}, F_{yi} are the forces acting on the wheel in the longitudinal and transverse directions of the wheel axis, a_x, a_y are the longitudinal and transverse accelerations of the COG, l_f, l_r, b_f, b_r describe the geometric characteristics of the vehicle, F_{res} is the total drag force, ρ is the air density, A_F is the cross-sectional area of the vehicle, C_d is the aerodynamic drag coefficient, c_{rr} is the rolling friction coefficient, g is the gravitational acceleration.

The steering angle distribution rule is as follows (δ_1, δ_2 are the left and right front wheel steering angles, respectively):

$$\begin{aligned} &\left(\delta_{dr} > 0\right), \delta_1 = \delta_{dr}, \delta_2 = \arctan\frac{\left(R - 0.5b_f\right)\tan\delta_{dr}}{R + 0.5b_f} \\ &\left(\delta_{dr} < 0\right), \delta_2 = \delta_{dr}, \delta_1 = \arctan\frac{\left(R - 0.5b_f\right)\tan\delta_{dr}}{R + 0.5b_f} \\ &\left(\delta_{dr} = 0\right), \delta_1 = \delta_2 = \delta_{dr} \end{aligned} \quad (3)$$

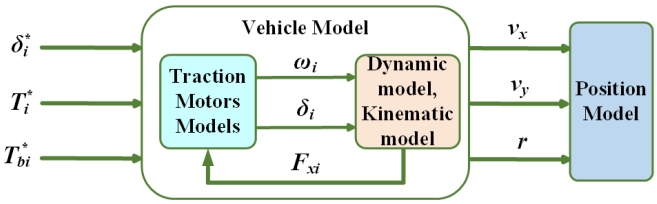

Fig. 1. Vehicle model structure.

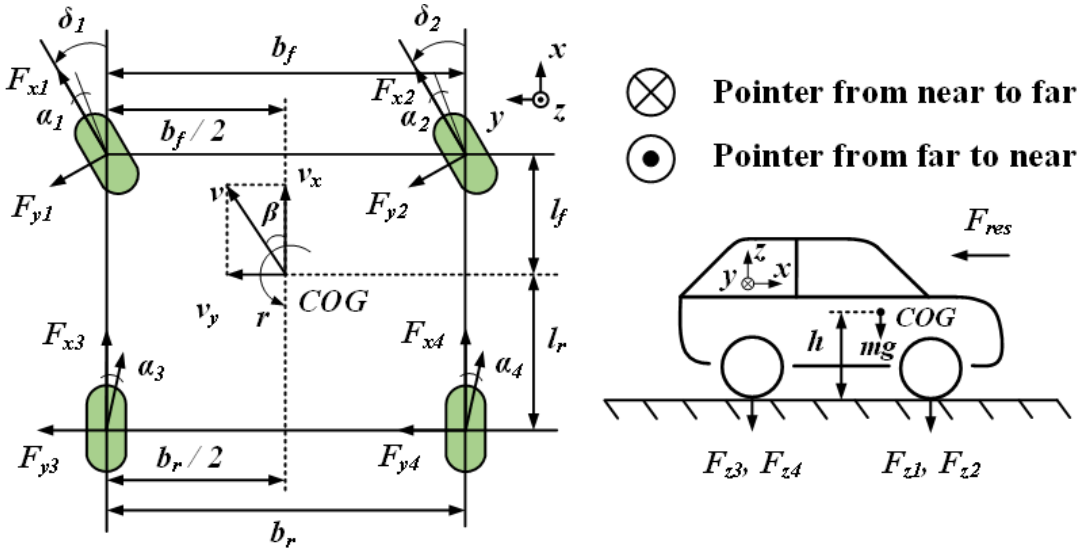

Fig. 2. Components acting on the vehicle and wheels.

The relationship $\mu-\lambda$ based on Burckhardt, shown in Figure 3, is given as follows [25]:

$$\mu_{res}=\left(c_1\left(1-e^{-c_2\lambda_{res}}\right)-c_3\lambda_{res}\right)e^{-c_4\lambda_{res}v}\left(1-c_5F_z^2\right) \quad (4)$$

where μ_{res} is the coefficient of friction, λ_{res} is the slip ratio, F_z is the normal force of the wheel on the road surface, c_1-c_5 are the road surface coefficients.

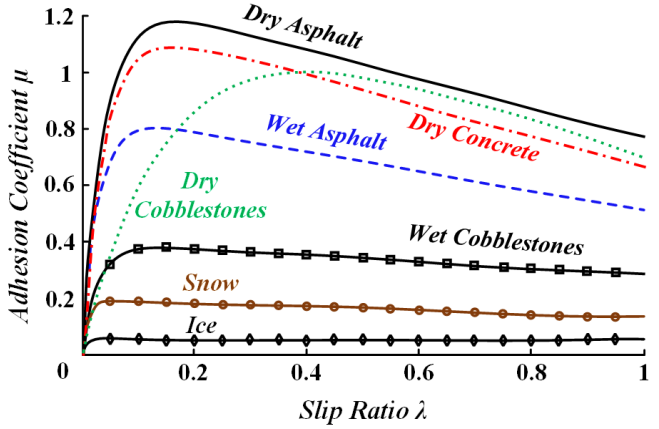

Fig. 3. Relationship between the coefficient of friction and the sliding ratio of the Burckhardt model.

The coefficient of friction at each wheel is as follows:

$$\mu_l=\mu_{res}\frac{\lambda_l}{\lambda_{res}},\mu_s=k_s\mu_{res}\frac{\lambda_s}{\lambda_{res}} \quad (5)$$

where μ_l, μ_s are the friction coefficients in the longitudinal and transverse directions of the wheel, λ_l, λ_s are the longitudinal and transverse slip ratios of the wheel, and k_s is the attenuation coefficient. The slip ratio is calculated as follows (R_{eff} is the effective wheel radius):

$$\lambda=\frac{\omega R_{eff}-v_x}{\max\left(\omega R_{eff},v_x\right)} \quad (6)$$

According to [26], the relationship between F_x and F_z is described as follows:

$$F_x=F_z\mu_{res}\left(\lambda_{res}\right) \quad (7)$$

According to [27], the four-wheel velocity is calculated as follows (β is the slip angle of body x).

$$\begin{cases}v_{s1}=v-r\left(0.5b_f-l_f\beta\right)\\ v_{s2}=v+r\left(0.5b_f-l_f\beta\right)\\ v_{s3}=v-r\left(0.5b_r-l_r\beta\right)\\ v_{s4}=v+r\left(0.5b_r-l_r\beta\right)\end{cases} \quad (8)$$

The force acting on the wheel is calculated according to the following formula:

$$\begin{cases}F_x=\left(\mu_{res}\frac{\lambda_l}{\lambda_{res}}\cos\alpha+\mu_{res}k_s\frac{\lambda_s}{\lambda_{res}}\sin\alpha\right)F_z\\ F_y=\left(-\mu_{res}\frac{\lambda_l}{\lambda_{res}}\sin\alpha+\mu_{res}k_s\frac{\lambda_s}{\lambda_{res}}\cos\alpha\right)F_z\end{cases} \quad (9)$$

According to [28], the magnitude of F_z is calculated as:

$$\begin{cases}F_{z1}=\left(k_{rx}-k_x\frac{a_x}{g}\right)\left(1-k_{fy}\frac{a_y}{g}\right)\\ F_{z2}=\left(k_{rx}-k_x\frac{a_x}{g}\right)\left(1+k_{fy}\frac{a_y}{g}\right)\\ F_{z3}=\left(k_{fx}+k_x\frac{a_x}{g}\right)\left(1-k_{ry}\frac{a_y}{g}\right)\\ F_{z4}=\left(k_{fx}+k_x\frac{a_x}{g}\right)\left(1+k_{ry}\frac{a_y}{g}\right)\end{cases} \quad (10)$$

with $k_{rx}=\frac{1}{2}mg\frac{l_r}{l}$, $k_{ry}=2\frac{h}{b_r}$, $k_{fx}=\frac{1}{2}mg\frac{l_f}{l}$, $k_{fy}=2\frac{h}{b_f}$, $k_x=\frac{1}{2}mg\frac{h}{l}$, and $l=l_f+l_r$.

B. Vehicle Transmission Model

For each wheel, the drive model is represented as follows:

$$T_d=\frac{K_m}{\tau_m s+1}T_d^* \quad (11)$$

where K_m is the motor amplification factor, τ_m is the time constant, and T_d is the driving torque:

$$T_d-R_{eff}F_x-k_bT_b=J_x\frac{d\omega}{dt} \quad (12)$$

Equation (12) is the moment balance equation for each wheel. In this case, J_x is the moment of inertia of the wheel and k_bT_b is the braking moment acting on the wheel axle.

C. Vehicle Dynamics Model

According to [29], the equation that expresses the relationship between vehicle kinematics and dynamics is as follows:

$$M\dot{v}+C\left(v\right)=\tau \quad (13)$$

where M, $C\left(v\right)$ are the inertial and Coriolis matrices, $\dot{v}$ is a vector, and τ is the torque that passes through the vehicle's center of gravity around the vertical axis.

The dynamic model showing the relationship between acceleration, velocity, and yaw rate of a typical vehicle is represented as follows:

$$\begin{cases} \dot{v}_x = a_x + rv_y \\ \dot{v}_y = a_y - rv_x \end{cases} \quad (14)$$

III. DESIGN OF SLIP RATIO OBSERVER

Figure 4 shows the control structure of the entire power distribution system. There, the slip ratio will be observed, and the vehicle model will be built on two software, Matlab Simulink and CarSim.

Deriving both sides of (6), we get:

$$\dot{\lambda} = \frac{\dot{v}_x \omega - v_x \dot{\omega}}{\omega^2 R_{eff}} \quad (15)$$

In straight motion, $\dot{v}_x = a_x$ and (15) is rewritten as follows:

$$\begin{aligned} \dot{\lambda} &= -\left(\frac{a_x}{R_{eff}\omega} + \frac{R_{eff}\omega - v_x}{R_{eff}} \frac{\dot{\omega}}{\omega} - \frac{\dot{\omega}}{\omega} \right) \\ &= -\frac{a_x}{R_{eff}\omega} - \lambda \frac{\dot{\omega}}{\omega} + \frac{\dot{\omega}}{\omega} \Rightarrow \dot{\lambda} = -\frac{a_x}{R_{eff}\omega} - \lambda \frac{\dot{\omega}}{\omega} + \frac{\dot{\omega}}{\omega} \end{aligned} \quad (16)$$

According to [30], a slip ratio estimator is proposed as follows:

$$\dot{\lambda} = -\frac{a_x}{R_{eff}\omega} - \hat{\lambda}\frac{\dot{\omega}}{\omega} + \frac{\dot{\omega}}{\omega} \quad (17)$$

The term $\dot{\omega}$ contains derivative components, so it is very sensitive to noise, causing instability or affecting the estimator's convergence. In this case, an estimator with an additional error feedback component between the actual and estimated acceleration is proposed as follows:

$$\dot{\hat{\lambda}} = -\frac{a_x}{R_{eff}\omega} - \hat{\lambda}\frac{\dot{\omega}}{\omega} + \frac{\dot{\omega}}{\omega} + k\left(\hat{\lambda}\right)\left(\dot{v}_x - \dot{\hat{v}}_x\right) \quad (18)$$

where $\dot{\hat{v}}_x = \mu g$, $\mu = \sigma_s \hat{\lambda}$, and $\sigma_s = 1$. Finally, the proposed force estimator structure is shown below.

$$\dot{\hat{\lambda}} = -\frac{a_x}{R_{eff}\omega} - \hat{\lambda}\frac{\dot{\omega}}{\omega} + \frac{\dot{\omega}}{\omega} + k\left(\hat{\lambda}\right)\left(a_x - \hat{\lambda} g\right) \quad (19)$$

To ensure the accuracy of the estimator λ, the coefficient $\hat{\lambda}$ must be chosen to ensure the convergence of the estimator. We obtain the derivative of both sides of the estimation error $\varepsilon(t) = \lambda - \hat{\lambda}$ as follows:

$$\dot{\varepsilon}(t) = \dot{\lambda} - \dot{\hat{\lambda}} \quad (20)$$

Replacing (16) and (19) into (20) we obtain:

$$\begin{aligned} \dot{\varepsilon}(t) &= -\frac{\dot{\omega}}{\omega}\varepsilon(t) - k\left(\hat{\lambda}\right)\left(a_x - \hat{\lambda} g\right) \\ &= -\left(\frac{\dot{\omega}}{\omega} + k\left(\hat{\lambda}\right) g\right)\varepsilon(t) - k\left(\hat{\lambda}\right)\left(a_x - \lambda g\right) \end{aligned} \quad (21)$$

To ensure convergence for the observer λ, then:

$$\frac{\dot{\omega}}{\omega} + k\left(\hat{\lambda}\right) g > 0 \Rightarrow k\left(\hat{\lambda}\right) > -\frac{\dot{\omega}}{\omega g} \quad (22)$$

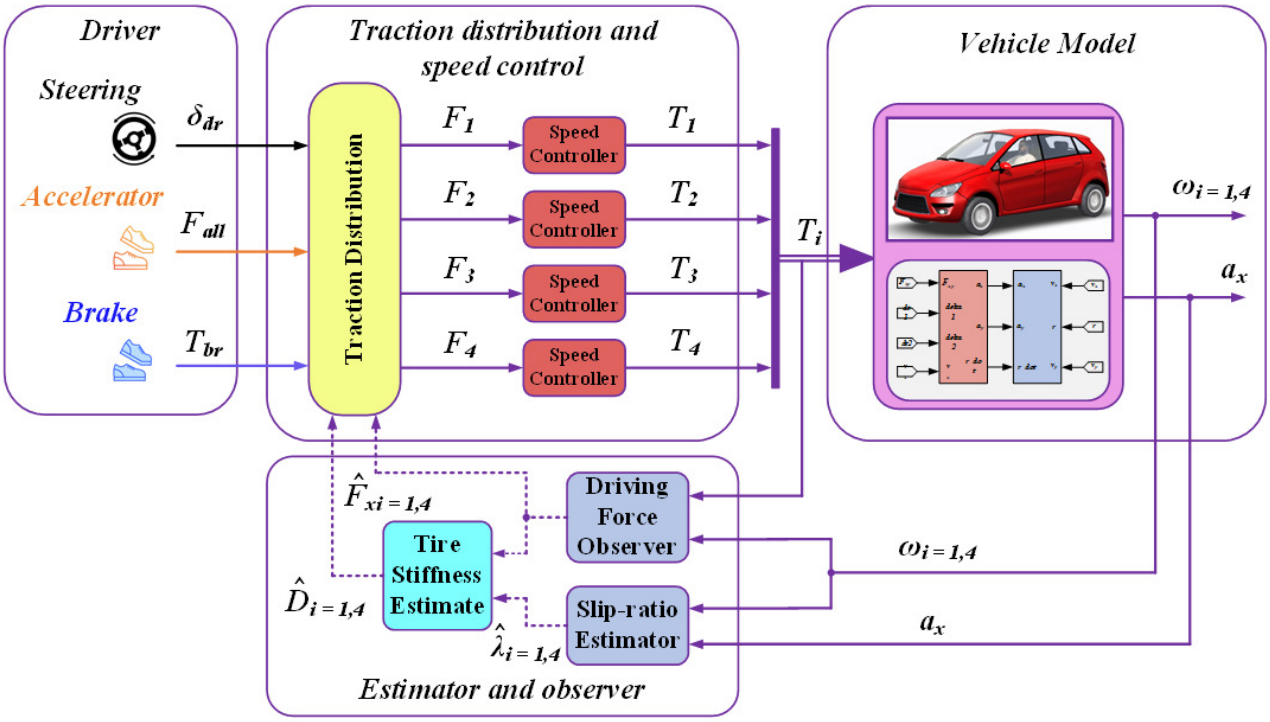

Fig. 4. Steering force distribution control structure.

IV. SIMULATION AND EVALUATION OF RESULTS

To observe the change in slip ratio and control quality of the power steering system, a snowy road surface with a low adhesion coefficient and a dry concrete road surface with a high adhesion coefficient are selected for testing. The procedure is described in Figure 5 and the simulation parameters are given in Table I.

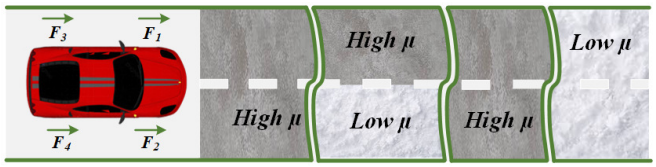

Fig. 5. Simulation scenario.

TABLE I. SIMULATION PARAMETERS

Quantity	Symbol	Value
Front and rear wheel distance	l	2.91 m
Front wheel axle and COG distance	l_f	1.105 m
Rear wheel axle and COG distance	l_r	1.895 m
Distance between the two front wheels	b_f	1.675 m
Distance between the two rear wheels	b_r	1.675 m
Vehicle mass	M	1270 kg
Effective wheel radius	R_{eff}	325 mm
Wind resistance surface area	A_F	2.2 m^2
Wheel moment of inertia	J_w	2 Nm
COG height from ground	h	0.54 m

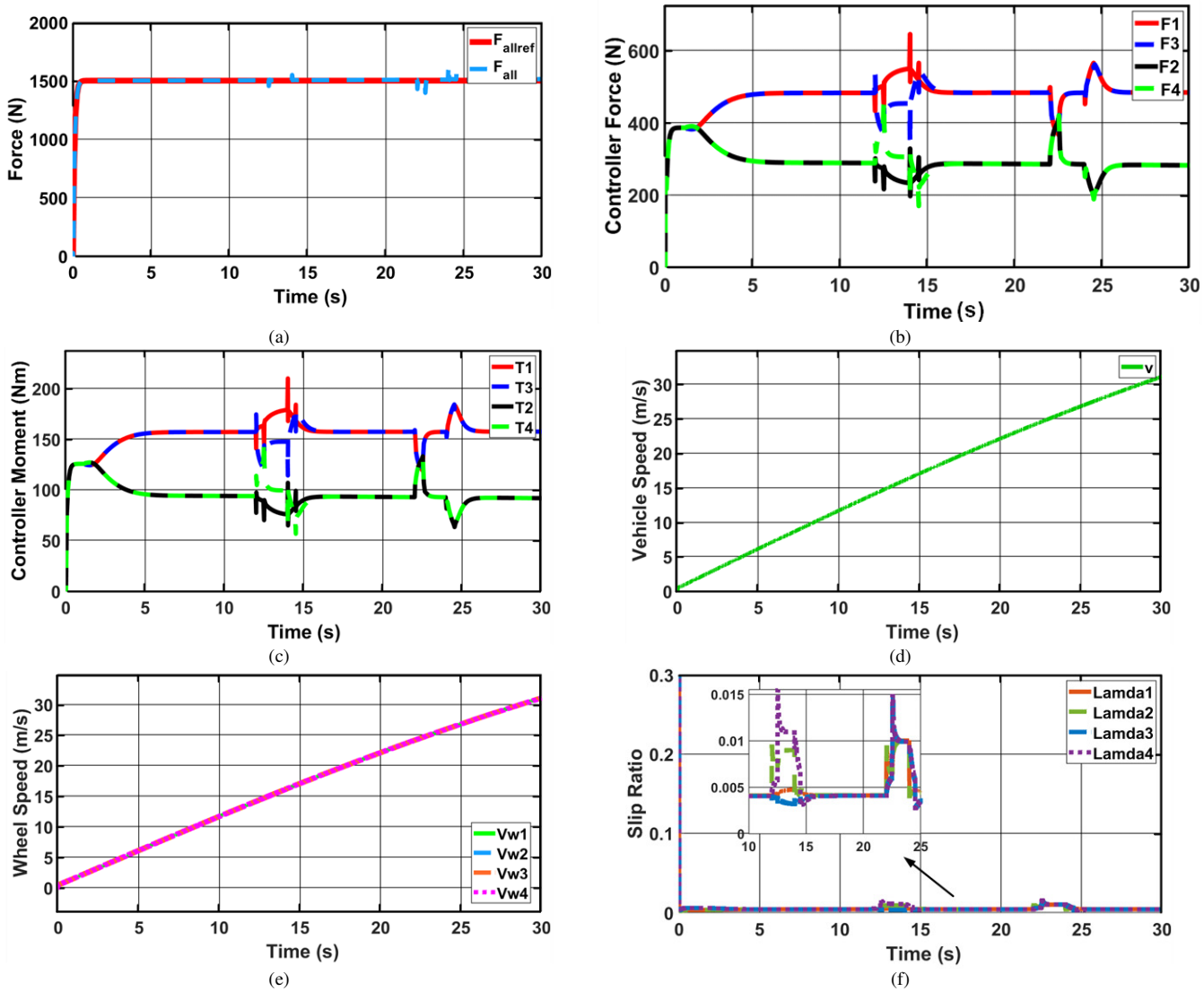

Fig. 6. Simulation results with a vehicle model on Matlab Simulink: (a) total applied traction; (b) traction force of each wheel; (c) moment of each wheel; (d) the vehicle's linear speed; (e) wheel speed; (f) four-wheel slip.

A. Simulation Results using a Vehicle Model Built on Matlab Simulink

Figure 6 describes the simulation results with the vehicle model designed in Matlab Simulink. Figure 6(a) shows that the total traction force closely follows the set traction force with a short settling time and changes when entering slippery road conditions. The traction forces and moments at each wheel in Figure 6(b) and Figure 6(c) have changed appropriately as the road conditions change to meet the requirements of the total traction force. We can see that the torque and traction force at the left wheels decrease and at the right wheels increase when entering slippery road conditions. However, when exiting the road after about 24 s and sliding on a concrete road with a significant friction coefficient, the torque and traction force at the wheels change in the opposite direction to maintain the total traction force at the set value. Figure 6(d) and Figure 6(e) show the speed of the vehicle and the wheels. The speed has gradually increased over time, and there is no significant effect when entering slippery road conditions. The wheel slip in Figure 6(f) is approximately 0. When entering a slippery road, there is a change, but it is minimal, so the vehicle maintains stability.

B. Simulation Results using a Vehicle Model Built on CarSim

The simulation results when building a vehicle model on CarSim are described in Figure 7. It can be seen that the total traction response in Figure 7(a) has closely followed the road conditions and has changed less than in Simulink. The vehicle and wheel speeds in Figure 7(d) and Figure 7(e) have also increased gradually and are less affected. The traction forces at each wheel in Figure 7(b) and the engine moment in Figure 7(c) change appropriately when the road conditions change to meet the total traction requirements. Figure 7(f) shows the slip ratio of the four wheels. Here, the slip ratio is about 0, and when entering slippery road conditions, the slip ratio fluctuates only slightly (about 0.008), which is much smaller than for the vehicle model in Simulink and does not affect the system's stability. Such high accuracy results demonstrate the accuracy of the CarSim software.

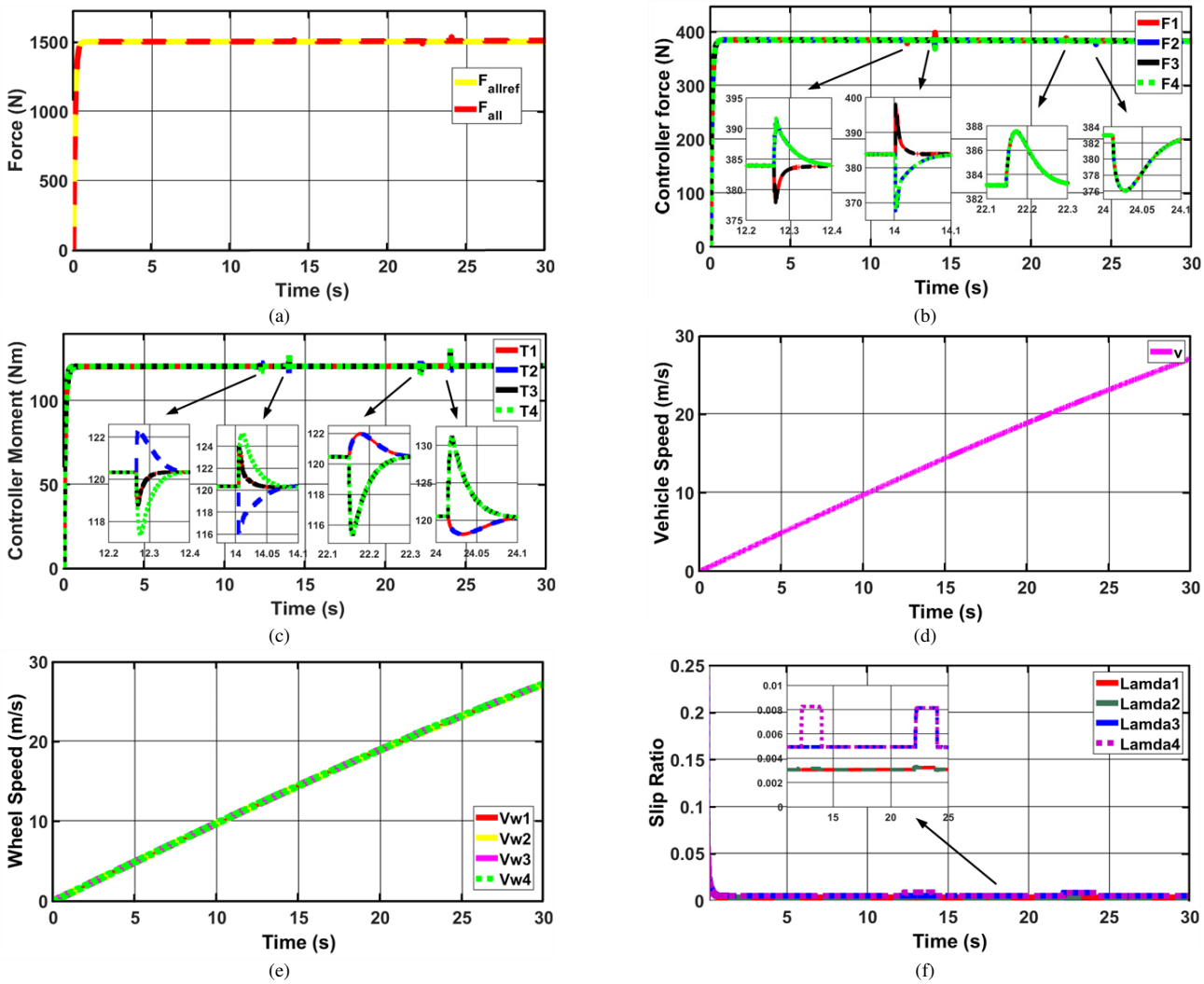

Fig. 7. Simulation results with a car model on CarSim: (a) total applied traction; (b) traction force of each wheel; (c) moment of each wheel; (d) the vehicle's linear speed; (e) wheel speed; (f) four-wheel slip.

V. CONCLUSION

This paper has studied and compared the effectiveness of two software, Matlab Simulink and CarSim, in simulating and optimizing the steering force control systems of Electric Vehicles (EVs). The author evaluated the accuracy, stability, feasibility, and efficiency of these two simulation tools by constructing a four-wheel vehicle model and applying a slip ratio observer. Such a comparison has provided valid insights and clarified the differences between the two software tools. The results show that CarSim provides detailed vehicle dynamics simulation capabilities and is closer to reality due to previously established and verified simulation parameters. Although Matlab Simulink is still limited in high accuracy, it is easy to adjust and the responses are good. The implementation of the slip ratio observer has further improved the accuracy and stability of the system. This study has opened up the potential for further applied research on EV stability control in the future.

ACKNOWLEDGMENT

We would like to thank the University of Transport and Communications for their financial support.

REFERENCES

[1] Y. Li, O. P. Adeleke, and X. Xu, "Methods and applications of energy saving control of in-wheel motor drive system in electric vehicles: A comprehensive review," *Journal of Renewable and Sustainable Energy*, vol. 11, no. 6, Nov. 2019, Art. no. 062701, https://doi.org/10.1063/1.5129070.

[2] R. Xiong, F. Sun, Z. Chen, and H. He, "A data-driven multi-scale extended Kalman filtering based parameter and state estimation approach of lithium-ion polymer battery in electric vehicles," *Applied Energy*, vol. 113, pp. 463–476, Jan. 2014, https://doi.org/10.1016/j.apenergy.2013.07.061.

[3] T. R. Hawkins, O. M. Gausen, and A. H. Strømman, "Environmental impacts of hybrid and electric vehicles—a review," *The International Journal of Life Cycle Assessment*, vol. 17, no. 8, pp. 997–1014, Sep. 2012, https://doi.org/10.1007/s11367-012-0440-9.

[4] G. Yin, R. Wang, and J. Wang, "Robust control for four wheel independently-actuated electric ground vehicles by external yaw-moment generation," *International Journal of Automotive Technology*, vol. 16, no. 5, pp. 839–847, Oct. 2015, https://doi.org/10.1007/s12239-015-0086-2.

[5] Y. Chen and J. Wang, "Adaptive Energy-Efficient Control Allocation for Planar Motion Control of Over-Actuated Electric Ground Vehicles," *IEEE Transactions on Control Systems Technology*, vol. 22, no. 4, pp. 1362–1373, Jul. 2014, https://doi.org/10.1109/TCST.2013.2287560.

[6] G. A. Magallan, C. H. De Angelo, and G. O. Garcia, "Maximization of the Traction Forces in a 2WD Electric Vehicle," *IEEE Transactions on Vehicular Technology*, vol. 60, no. 2, pp. 369–380, Feb. 2011, https://doi.org/10.1109/TVT.2010.2091659.

[7] G. Boztas, M. Yildirim, and O. Aydogmus, "Design and Analysis of Multi-Phase BLDC Motors for Electric Vehicles," *Engineering, Technology & Applied Science Research*, vol. 8, no. 2, pp. 2646–2650, Apr. 2018, https://doi.org/10.48084/etasr.1781.

[8] A. Khadhraoui, T. Selmi, and A. Cherif, "Energy Management of a Hybrid Electric Vehicle," *Engineering, Technology & Applied Science Research*, vol. 12, no. 4, pp. 8916–8921, Aug. 2022, https://doi.org/10.48084/etasr.5058.

[9] K. Cherif, A. Sahbani, and K. B. Saad, "Performance Evaluation of PI and Sliding Mode Control for PMSM in Applications for Electric Vehicles," *Engineering, Technology & Applied Science Research*, vol. 14, no. 4, pp. 15464–15470, Aug. 2024, https://doi.org/10.48084/etasr.7172.

[10] V. H. Nguyen, "Speed Control of Electric Vehicles Base on PID Robust Controller," *Transport and Communications Science Journal*, vol. 75, no. 8, pp. 2154–2166, Oct. 2024, https://doi.org/10.47869/tcsj.75.8.1.

[11] V. H. Nguyen and T. H. Vo, "Optimising torque for three-disc afpmsm in electric vehicles using bp_ann and anfis algorithms," *Transport and Communications Science Journal*, vol. 76, no. 1, pp. 1–15, Jan. 2025, https://doi.org/10.47869/tcsj.76.1.1.

[12] Y. Ge and C. Chang, "Torque distribution control for electric vehicle based on traction force observer," in *2011 IEEE International Conference on Computer Science and Automation Engineering*, Shanghai, China, 2011, pp. 371–375, https://doi.org/10.1109/CSAE.2011.5952490.

[13] D. Savitski *et al.*, "Improvement of traction performance and off-road mobility for a vehicle with four individual electric motors: Driving over icy road," *Journal of Terramechanics*, vol. 69, pp. 33–43, Feb. 2017, https://doi.org/10.1016/j.jterra.2016.10.005.

[14] Z. Lipeng, L. Shuaishuai, Y. Haojie, R. Changan, and L. Shaohua, "Centralized and distributed coupling traction control of electric vehicles on split ramps," *Mechanism and Machine Theory*, vol. 179, Jan. 2023, Art. no. 105098, https://doi.org/10.1016/j.mechmachtheory.2022.105098.

[15] H. Jing, F. Jia, and Z. Liu, "Multi-Objective Optimal Control Allocation for an Over-Actuated Electric Vehicle," *IEEE Access*, vol. 6, pp. 4824–4833, 2018, https://doi.org/10.1109/ACCESS.2017.2788941.

[16] S. Fallah, A. Khajepour, B. Fidan, S.-K. Chen, and B. Litkouhi, "Vehicle Optimal Torque Vectoring Using State-Derivative Feedback and Linear Matrix Inequality," *IEEE Transactions on Vehicular Technology*, vol. 62, no. 4, pp. 1540–1552, May 2013, https://doi.org/10.1109/TVT.2012.2232947.

[17] Y. Li, H. Deng, X. Xu, and W. Wang, "Modelling and testing of in-wheel motor drive intelligent electric vehicles based on co-simulation with Carsim/Simulink," *IET Intelligent Transport Systems*, vol. 13, no. 1, pp. 115–123, Oct. 2019, https://doi.org/10.1049/iet-its.2018.5047.

[18] N. Jiang and R. Qiu, "Modelling and Simulation of Vehicle ESP System Based on CarSim and Simulink," *Journal of Physics: Conference Series*, vol. 2170, no. 1, Feb. 2022, Art. no. 012032, https://doi.org/10.1088/1742-6596/2170/1/012032.

[19] K. Nam, Y. Hori, and C. Lee, "Wheel Slip Control for Improving Traction-Ability and Energy Efficiency of a Personal Electric Vehicle," *Energies*, vol. 8, no. 7, pp. 6820–6840, Jul. 2015, https://doi.org/10.3390/en8076820.

[20] Z. Shuai, H. Zhang, J. Wang, J. Li, and M. Ouyang, "Combined AFS and DYC Control of Four-Wheel-Independent-Drive Electric Vehicles over CAN Network with Time-Varying Delays," *IEEE Transactions on Vehicular Technology*, vol. 63, no. 2, pp. 591–602, Feb. 2014, https://doi.org/10.1109/TVT.2013.2279843.

[21] C. Hu, R. Wang, and F. Yan, "Integral Sliding Mode-Based Composite Nonlinear Feedback Control for Path Following of Four-Wheel Independently Actuated Autonomous Vehicles," *IEEE Transactions on Transportation Electrification*, vol. 2, no. 2, pp. 221–230, Jun. 2016, https://doi.org/10.1109/TTE.2016.2537046.

[22] Y. X. Chen, "Research on direct yaw moment control of distributed drive electric vehicle," Ph.D. dissertation, Jilin University, Changchun, China, 2013.

[23] R. Hou, L. Zhai, and T. Sun, "Steering Stability Control for a Four Hub-Motor Independent-Drive Electric Vehicle with Varying Adhesion Coefficient," *Energies*, vol. 11, no. 9, Sep. 2018, Art. no. 2438, https://doi.org/10.3390/en11092438.

[24] H. He, J. Peng, R. Xiong, and H. Fan, "An Acceleration Slip Regulation Strategy for Four-Wheel Drive Electric Vehicles Based on Sliding Mode Control," *Energies*, vol. 7, no. 6, pp. 3748–3763, Jun. 2014, https://doi.org/10.3390/en7063748.

[25] T. Vo-Duy, M. C. Ta, B.-H. Nguyễn, and J. P. F. Trovão, "Experimental Platform for Evaluation of On-Board Real-Time Motion Controllers for Electric Vehicles," *Energies*, vol. 13, no. 23, Dec. 2020, Art. no. 6448, https://doi.org/10.3390/en13236448.

[26] R. de Castro, R. E. Araújo, and D. Freitas, "Wheel Slip Control of EVs Based on Sliding Mode Technique With Conditional Integrators," *IEEE*

Transactions on Industrial Electronics, vol. 60, no. 8, pp. 3256–3271, Aug. 2013, https://doi.org/10.1109/TIE.2012.2202357.

[27] U. Kiencke and L. Nielsen, "Vehicle Modelling," in *Automotive Control Systems: For Engine, Driveline, and Vehicle*, 2nd ed. Berlin/Heidelberg, Germany: Springer, 2005, pp. 301–349, https://doi.org/10.1007/3-540-26484-1_8.

[28] V.-D. Thanh and M. C. Ta, "A Universal Dynamic and Kinematic Model of Vehicles," in *2015 IEEE Vehicle Power and Propulsion Conference*, Montreal, Canada, 2015, pp. 1–6, https://doi.org/10.1109/VPPC.2015.7352889.

[29] U. Kiencke and L. Nielsen, *Automotive Control Systems: For Engine, Driveline, and Vehicle*. Warrendale, PA, USA: Society of Automotive Engineering, Incorporated, 2000.

[30] S. Li and T. Kawabe, "Slip Suppression of Electric Vehicles Using Sliding Mode Control Method," *Intelligent Control and Automation*, vol. 4, no. 3, pp. 327–334, Aug. 2013, https://doi.org/10.4236/ica.2013.43038.